Influence of background size, luminance and eccentricity on different adaptation mechanisms

Alejandro H. Gloriani [a], Beatriz M. Matesanz [a], Pablo A. Barrionuevo [b], Isabel Arranz [a], Luis Issolio [b], Santiago Mar [a], Juan A. Aparicio [a,*]

[a] Departamento de Óptica, Universidad de Valladolid, P. Belén 7, 47011 Valladolid, Spain
[b] Departamento de Luminotecnia, Luz y Visión, Universidad Nacional de Tucumán, Instituto de Investigación en Luz, Ambiente y Visión, CONICET-UNT, Avenida de Independencia 1800, 4000 Tucumán, Argentina

ABSTRACT

Mechanisms of light adaptation have been traditionally explained with reference to psychophysical experimentation. However, the neural substrata involved in those mechanisms remain to be elucidated. Our study analyzed links between psychophysical measurements and retinal physiological evidence with consideration for the phenomena of rod-cone interactions, photon noise, and spatial summation. Threshold test luminances were obtained with steady background fields at mesopic and photopic light levels (i.e., 0.06–110 cd/m^2) for retinal eccentricities from 0° to 15° using three combinations of background/test field sizes (i.e., 10°/2°, 10°/0.45°, and 1°/0.45°). A two-channel Maxwellian view optical system was employed to eliminate pupil effects on the measured thresholds. A model based on visual mechanisms that were described in the literature was optimized to fit the measured luminance thresholds in all experimental conditions. Our results can be described by a combination of visual mechanisms. We determined how spatial summation changed with eccentricity and how subtractive adaptation changed with eccentricity and background field size. According to our model, photon noise plays a significant role to explain contrast detection thresholds measured with the 1/0.45° background/test size combination at mesopic luminances and at off-axis eccentricities. In these conditions, our data reflect the presence of rod-cone interaction for eccentricities between 6° and 9° and luminances between 0.6 and 5 cd/m^2. In spite of the increasing noise effects with eccentricity, results also show that the visual system tends to maintain a constant signal-to-noise ratio in the off-axis detection task over the whole mesopic range.

© 2016 Elsevier Ltd. All rights reserved.

1. Introduction

Light adaptation allows visual detection in a large dynamic range of ambient light levels, which can span more than eight orders of magnitude (Hood & Finkelstein, 1986). Threshold versus intensity (*tvi*) functions have been traditionally used by psychophysicists to study adaptation to varying light levels (Barlow, 1965; Donner, 1992; Shapley & Enroth-Cugell, 1984). In these experiments, the effect of adapting backgrounds was quantified with a just-detectable probe flash superimposed on the background. The switching between rod and cone mediation is one adaptation mechanism that can be described with a *tvi* curve. Also, changes in spatial, temporal and spectral characteristics of the stimulation allowed determination of the laws of neural adaptation based on these curves. Early studies typically ascribed behavioral findings to two main adaptation mechanisms: (1) Gain control mechanisms that establish a proportionality between the increments (or decrements) of impulse rate variation in retinal ganglion cells and increments (or decrements) in the retinal illumination (Shapley & Enroth-Cugell, 1984); and (2) Subtractive mechanisms partially eliminate the signal corresponding to steady luminance, reducing it to a lower effective value.

Based on psychophysical experiments, other adaptation mechanisms, such as contrast gain and non-linear processing stages (including saturation, noise and spatial summation) have been considered (Barrionuevo, Colombo, & Issolio, 2013; Cao & Pokorny, 2010; Murray & Plainis, 2003; Rieke & Rudd, 2009; Smith & Pokorny, 2003; Snippe, Poot, & van Hateren, 2000, 2004; Wilson, 1997). Saturation is understood as a non-linear process caused by the limited dynamic range of retinal neurons. Detection experiments are also thought to be affected by noise. The effect of

noise was found to be significant at low light levels, especially with brief and small backgrounds in peripheral retina (Bauer, Frumkes, & Holstein, 1983; Bauer, Frumkes, & Nygaard, 1983). Spatial summation has also been traditionally studied using psychophysical approaches (Barlow, 1958; Redmond, Zlatkova, Vassilev, Garway-Heath, & Anderson, 2013) and its changes are explained by an increasing receptive field size with eccentricity. Modern physiology has also contributed to this type of study; e.g., functional magnetic resonance imaging methods estimated that the receptive field size increases with eccentricity in humans whereas other physiological studies provided a quantitative description of the spatial receptive fields in primates and rats (Croner & Kaplan, 1994; Dumoulin & Wandell, 2008; Heine & Passaglia, 2011).

Recent advances in understanding the underlying physiological mechanisms of adaptation processes have provided deeper insight into this field. Gain control mechanisms located at outer retina (photoreceptors) and inner retina (ganglion cell) levels have been characterized (Dunn et al., 2006; Dunn, Lankheet, & Rieke, 2007). Freeman, Graña, and Passaglia (2010) proposed a novel, fast and high-sensitivity luminance gain control mechanism whose changes followed Weber's law. This physiological mechanism was said to reside within the inner retinal network and not in the photoreceptors. In order to understand this mechanism, very recent works have focused on the interactions between photoreceptors, horizontal cells and bipolar cells (Joselevitch & Kamermans, 2013; Thoreson & Mangel, 2012). According to these authors, post-synaptic mechanisms at bipolar cell dendrites play a significantly important role by modulating the strength of their response to light. These mechanisms eventually extend the range of ambient luminances our visual system can be adapted. On the other hand, Tyler and Liu found that luminance variation of a small background pedestal does not affect the state of the gain control mechanism as much as it is affected by large background fields (Tyler & Liu, 1996). Concerning adaptation to contrast, Demb (2008) suggested that bipolar, amacrine and ganglion cells were involved in a complex process through synaptic and intrinsic mechanisms whose aim was to enhance contrast detection. The discussion concerning the physiological origin of luminance and background adaptation mechanisms is ongoing (Demb, 2008; Freeman et al., 2010) although the most recent studies have suggested that both mechanisms depend, in part, on a common synaptic process (Jarsky et al., 2011).

A subtractive mechanism was initially hypothesized as the result of feedback between cones and horizontal cells (Wilson, 1997). Wilson's assumptions and conjectures about this mechanism seem to have been corroborated by physiologists in the study of different fish species. For example, Klaassen, Fahrenfort, and Kamermans (2012) showed that gap junction proteins can also function as hemichannels that mediate a sign inverting inhibitory synaptic signal from horizontal cells to cones via an ephaptic mechanism. Furthermore, VanLeeuwen, Fahrenfort, Sjoerdsma, Numan, and Kamermans (2009) verified the existence of a lateral gain control mechanism in the horizontal cells of goldfish retinas that modulates the synaptic gain of cones and is finally visible in ganglion cell responses.

All these advances have renewed interest in relating psychophysical experiments with underlying physiological mechanisms. As an example, the work performed by Freeman et al. (2010) offers an explanation for the psychophysical evidence that low contrast stimuli can activate a local adaptation luminance mechanism in the mammalian retina, according to the authors. On the other hand, starting from psychophysics, Stockman, Petrova, and Henning (2014) proposed a physiologically relevant model of the chromatic and brightness pathways.

Concerning the background adaptation luminance, vision is mediated by cones at bright background light levels (photopic

vision), while rods alone are working at dim background light levels (scotopic vision). The mesopic light range covers four orders of magnitude, approximately, between the photopic and scotopic ranges. Under mesopic background light levels, both rods and cones are simultaneously activated (Buck, 2004, 2014; Zele & Cao, 2015). In addition to rod and cone spectral domains being relatively shifted, their density distributions across the retina are different (Curcio, Sloan, Kalina, & Hendrickson, 1990; Osterberg, 1935). Rod and cone temporal and spatial contrast sensitivity functions (Stockman & Sharpe, 2006), which are directly related to their receptive field characteristics, differ as well. Classic studies on *tvi* functions have shown that backgrounds of small size, designed to be detected by rods, affect contrast thresholds when the test is detected by cones, and stimuli designed to be detected by cones affect contrast thresholds when the test is detected by rods (Buck, Peeples, & Makous, 1979; Latch & Lennie, 1977; Temme & Frumkes, 1977). A conclusion from these studies is lateral involvement of rods is necessary for the increase in cone thresholds. Since this effect seems to happen only for small backgrounds, in mesopic conditions where rods and cones work together it is important to consider the effect of stimulus size. In conclusion, rod and cone signals interact and their light adaptation mechanisms change with intensity, eccentricity and stimuli sizes.

Furthermore, all types of photoreceptors, bipolar and ganglion cells change their densities and physiological properties in a significant way across the retina (e.g. Crook, Packer, Troy, & Dacey, 2014; Curcio et al., 1990; Garway-Heath, Caprioli, Fitzke, & Hitchings, 2000). Therefore, in order to reach a deeper insight into the retinal behavior, particularly in the whole perifoveal region, it is necessary to perform measurements at different retinal locations.

Psychophysical light adaptation measurements should reflect all of these physiological features. Because of the anatomical and physiological rod-cone differences, the study of mesopic vision is challenging. In this work, we report *tvi* measurements under several conditions, covering mesopic (0.06 cd/m^2) to low photopic (110 cd/m^2) adapting light levels, foveal (0°) to extrafoveal (15°) eccentricities, and three combinations of stimuli sizes, one of them including a 1° background field size. Traditional studies using large backgrounds, focused on overall retinal mechanisms. In this sense, it is particularly interesting to understand the adaptation-to-light mechanisms involved in a specific retinal position, a small background allowing for the study of this condition. Our study analyzed the following questions. (1) Is it possible to explain luminance thresholds under such diverse experimental conditions, particularly in off-axis retinal locations? (2) To what extent does a small stimulus size affect the adaptation process? (3) What links can be established between the psychophysical measurements and the underlying physiological mechanisms? The third question is probably the most important question. Despite the complexity that could arise from the wide span of our experimental conditions, we developed a physiological- and psychophysical-based model that successfully fitted our results. Our model was shown to be useful for analyzing the effects of light intensity, eccentricity and stimuli sizes on light adaptation mechanisms.

2. Methods

2.1. Experimental set-up

A two-channel Maxwellian view optical system was employed, which was previously described elsewhere (Matesanz et al., 2011). Briefly, two concentric beams reach the observer's pupil: a background beam (with luminance L_b) and a probe (with luminance ΔL). Henceforth, we will refer to the spatial region where both beams are combined ($L_b + \Delta L$) as the *test*. The angular size of the

test is the same as the probe. At the observer's pupil, the background field can subtend eligible angles between 1° and 10°. The probe subtends eligible angles between 0.45° and 2°. The light source employed in this work was an incandescent halogen lamp with a color temperature of approximately 3000 K. Several shutters controlled the stimulus and the fixation test exposure times as well as the delay between them. The uncertainty in the timing control was measured with a photodiode and was less than 1 ms. Neutral density filters controlled the luminance of the background and the probe beams stepped in 0.1 log units. The entire instrument was controlled by a computer. Luminances were measured by a Spectra Pritchard 1980 luminance meter. Henceforth, all the luminance data are given in photopic cd/m^2. During measurements, the observer's head was fixated to the set-up with use of a bite bar made of dental compound. The observer's face was illuminated with infrared LEDs (830 nm) and the pupil was imaged with a CCD camera in

order to verify that its size was greater than the imaged filament (2×1 mm^2). Before any trial or measurement, the observer's pupil was centered on the plane containing the two overlapped images of the filament (one for each beam).

2.2. Subjects

The tenets of the Declaration of Helsinki were followed. Three of the authors were participants in the study (AG, IA, and BM) with ages 27 years, 38 years and 40 years, respectively. All participants passed an ophthalmological examination including refraction, ocular media, and fundus assessment. No pathologies or ocular opacities were observed. The best optical refraction for far distance was employed in all cases in order to obtain visual acuities logMar 0.0 or better. All measurements were performed on the temporal retina of the right eye while the left eye was occluded.
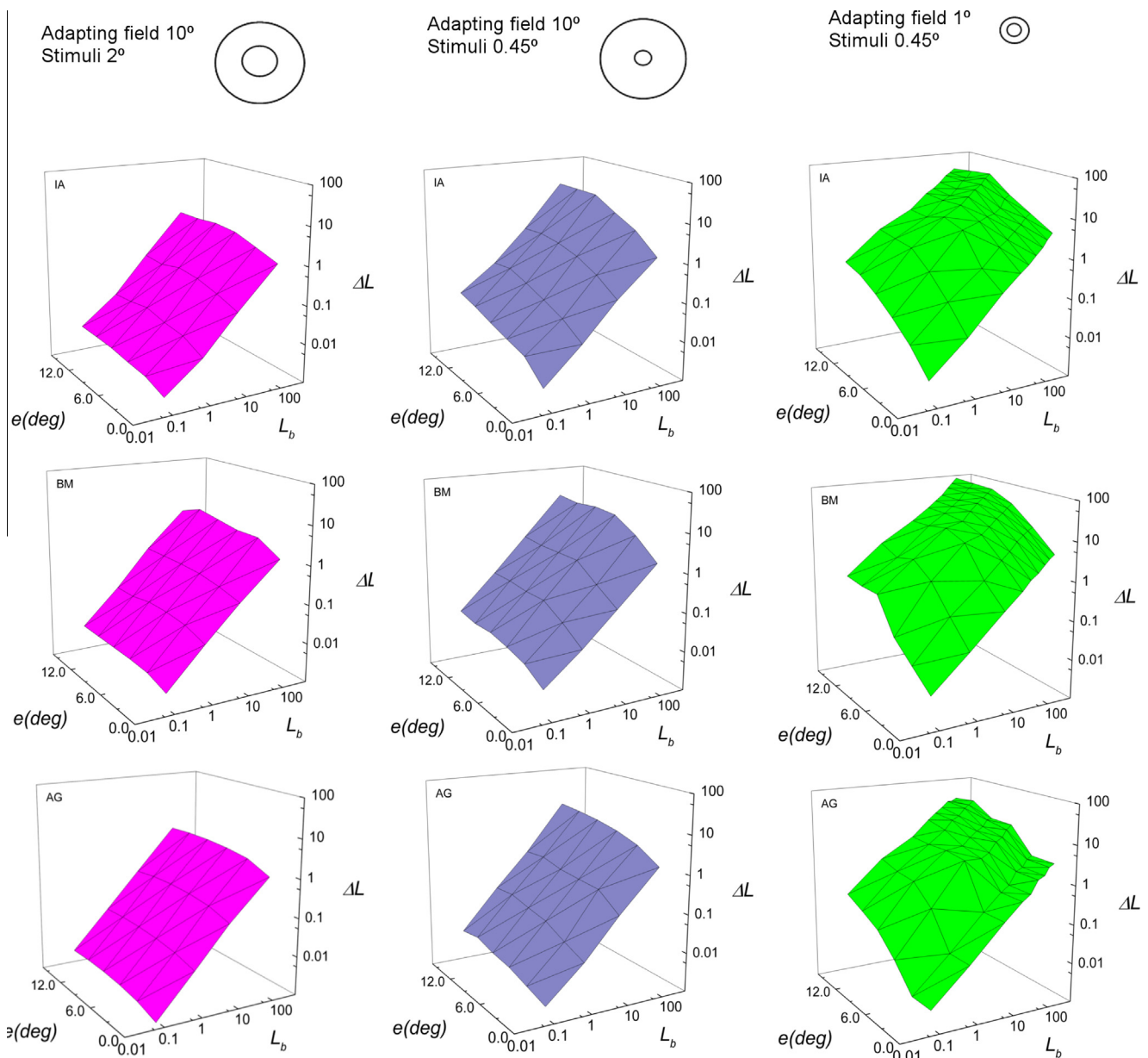

Fig. 1. Incremental threshold ΔL as a function of background luminance L_b (both in log scale) and the eccentricity e (°), for the three subjects (IA, BM and AG) under the three background/test field size conditions. ΔL and L_b are expressed in photopic cd/m^2. The maximum standard deviation for the experimental measurements was ± 0.15 log units.
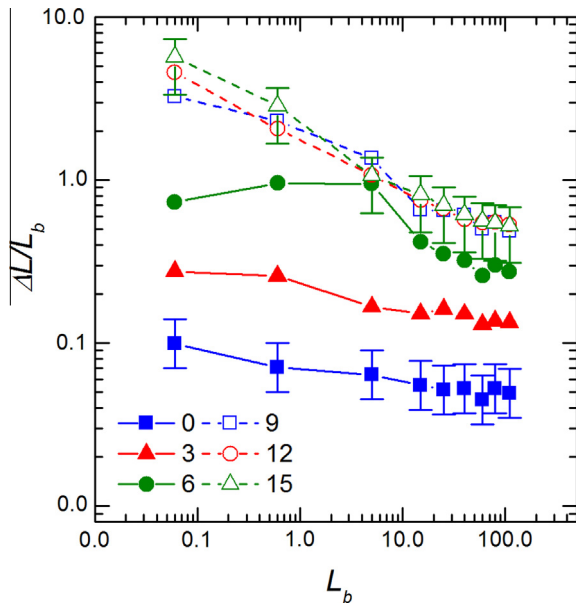
Fig. 2. Mean Weber contrast, $\Delta L/L_b$, for the three subjects as a function of L_b (in log scale) and for a background field of 1°. Data corresponding to all measured eccentricities are shown with different symbols and lines. Error bars represent the 95% confidence interval. For the sake of clarity, the error bars are only shown for 0° and 15°.

2.3. Procedure and measurements

Before measurements were obtained, the observers were adapted to darkness (5×10^{-6} cd/m², 1.43×10^{-5} scotopic trolands) for 30 min. Then, they adapted to the background luminance, L_b, for 10 min. After this adaptation, the probe was added to the background for 40 ms. The same temporal sequence was used as in our previous study (Fig. 2b, Matesanz et al., 2011). The observer's task was to report whether they detected the probe or not. The inter-stimulus interval (ISI) was 10 s for all of the background luminance levels, except for $L_b \geqslant 15$ cd/m² where the ISI was increased to 30 s in order to avoid afterimages (Adelson, 1982). In all cases, the subject's fixation was maintained on the proper fixation mark during light adaptation and during measurements. The foveal measurement fixation test consisted of four dim red fixation points in a diamond configuration whereas, for extrafoveal measurements, a single dim fixation point was employed. In all cases, tiny light emitting diodes (LEDs, central wavelengths at 630 nm) were used.

A limits method was employed for all measurements. In this method a staircase procedure is employed. A series begins with a stimulus intensity below the threshold, then the stimulus intensity is increased until it reaches the upper limit. Threshold for this series is estimated as the midpoint between the stimulus intensities for the last NO response and the first YES response. Then a series begins with stimulus intensity at the upper limit, so the stimulus intensity is decreased until it reaches the lower limit. On each trial the subject answers whether he/she can perceive the stimulus. Threshold for this series is estimated as the midpoint between the stimulus intensities of the last YES response and the first NO response. Runs may be performed ascending and descending in a random way Threshold is finally estimated as the average of the previously calculated midpoints, always being an equal number of ascending and descending staircases. In addition, in the mesopic range, the results were compared with the constant stimuli method. In these cases, a preliminary estimation of the luminance threshold was obtained with the limits method. Five probe luminances near the estimated threshold were repeated randomly 20

Table 1
Background and test field sizes and the background luminances employed in this study. All conditions were measured for the three observers in eccentricities from 0° to 15° in steps of 3°.

Background/test field sizes	L_b (in photopic cd/m²)
10°/2°	0.06, 0.6, 5, 60
10°/0.45°	0.06, 0.6, 5, 60
1°/0.45°	0.06, 0.6, 5, 15, 25, 40, 60, 110

times each. Afterwards, the final threshold, ΔL, was obtained from the psychometric curve. Differences between this value and the previously obtained value by the limits method were, in the most unfavorable case, lower than 0.15 log units.

For the three observers, measurements were performed with three different combinations of background and test beam sizes, according to the values shown in Table 1. The first column of this table shows the combination of field sizes and the second column shows the background luminances employed. The scotopic retinal illuminances (in scot. trolands) can be simply obtained by multiplying the photopic luminances (in phot. cd/m²) by the filament area (2 mm²) and by the scotopic to photopic ratio (S/P) which is 1.43 for our halogen incandescent lamp at 3000 K. All measurements were carried out for 0°, 3°, 6°, 9°, 12° and 15° of eccentricity (with respect to fixation).

For background luminances $L_b \leqslant 5$ cd/m², pupil diameters were around or greater than 4 mm for all subjects. This is the luminance that is considered to be the mesopic-to-photopic transition luminance. For greater L_b values, a mydriatic was employed (tropicamide 1%, Colircusi Alcon) in order to avoid pupil effects on retinal illumination. In these cases pupil diameters were always near or greater than 7 mm.

3. Results

In Fig. 1 the measured incremental thresholds, ΔL, are plotted as a function of the background luminance, L_b, (both in log scale), and eccentricity, e, (°) for the three subjects (IA, BM and AG) and for the three combinations of background/test field sizes. The incremental thresholds increased with background luminance for all subjects, all eccentricities and either test or background decreases in size. For a 10°/2° combination (left column of pictures), a fairly good linear relation was observed between them for all eccentricities (Weber's law). When these data were fitted using linear regression, the slopes ranged from 0.94 ± 0.06 in the fovea to 0.98 ± 0.06 at 15° eccentricity (95% confidence interval) with $R^2 > 0.98$ in all cases. When the test size was reduced to 0.45°, while keeping the background field size 10° (central column), this linear trend was maintained, but with higher incremental thresholds. The effect of reducing the test size was more marked for greater eccentricities.

When the background field was reduced to 1° and the test size was 0.45° (right column), the typical linear relation between incremental thresholds and background luminances disappeared, particularly in the mesopic-to-photopic transition (around 5 cd/m²) and for higher eccentricities ($\geqslant 6°$). From the behavioral point of view, we can conclude that Weber's law was fulfilled for 10° background field sizes, but not for 1° background field sizes. In order to check this point, we plotted the Weber contrast, $\Delta L/L_b$, as a function of L_b (in log scale) for 1° background fields for all considered retinal eccentricities (Fig. 2). Since the functional behavior was very similar for the three subjects, the data were averaged. As observed, Weber's contrast decreases slightly in 0°, 3° and 6° for all background luminances, although changes are lower than the 95% confidence error bar. Weber's law was clearly not satisfied between 9° and 15° (dashed lines in Fig. 2).

4. Model

A model was designed to calculate ΔL-values as a function of background luminance, eccentricity, and for the three different background/test field size combinations (Eq. (1)). This model contained adaptation and non-linear stages as suggested by classical psychophysical models (Adelson, 1982; Hayhoe, Benimoff, & Hood, 1987; Hayhoe, Levin, & Koshel, 1992; Snippe et al., 2000; Wilson, 1997). However these classical models needed to be updated based on new physiological findings about adaptation processes. Our model took into account such new evidence and could explain adaptation for a wide span of experimental conditions.

4.1. Mechanisms included in the model

Below we describe the different mechanisms that were considered. Note that optical effects, such as prereceptoral spectral transmittance or scattering in the subject's ocular media, have not been considered, however, their effect on *tvi* curves should be negligible because of the age of our participants. Concerning the light source and its spectral distribution, we focused our interest on the performance of the visual system under a typical halogen incandescent light source. Eq. (1) is the complete expression of our model, where L_T and L_b represent the test and background luminances, respectively; G_c is the contrast gain; $R(L_b)$ is the saturation response to background with σ and n representing the half-saturation constant and the Hill constant, respectively (Naka & Rushton, 1966); C_n, is the minimum Weber contrast; N represents a visual noise term; and S represents the subtractive mechanism. The mathematical details of the model are shown in the Appendix A.

$$\Delta L = \left(\frac{\sigma_T'^{\,n}}{\frac{1}{\left[\frac{C_n R(L_b)}{G_c}\right]+R(L_b)}-1} \right)^{1/n} + S + N - L_b \qquad (1)$$

4.1.1. Contrast gain

Contrast gain is defined as the ratio of a change in visual response to a contrast change in the stimulation. It usually increases with background field luminance and it is different for cones and rods (Cao & Pokorny, 2010; Purpura, Kaplan, & Shapley, 1988). In the past, Murray and Plainis (2003) provided experimental data on contrast gain for different adaptation luminances, eccentricities, and spatial frequencies.

4.1.2. Subtractive mechanism

Based on the feedback existing between cones and horizontal cells (Wilson, 1997), the subtractive mechanism tends to reduce the effect of the background luminance as well as the necessary ΔL-values to detect the stimulus. Therefore, this mechanism has a more significant influence in the photopic range in which cones show the largest contribution to test detection (Raphael & Macleod, 2011).

4.1.3. Gain controls

Gain control is defined as the change in response gain of the retinal system under a luminance change (Shapley & Enroth-Cugell, 1984). It tends to decrease as the adaptation luminance increases in the photopic range (Rieke & Rudd, 2009). Dunn, Doan, Sampath, and Rieke (2006), Dunn et al. (2007) found, in physiological studies, different gain controls for cones and rods. According to these authors, the main adaptation site was placed at the ganglion cells under light levels similar to those employed in this work. Furthermore, in photopic levels, a molecular adaptation mechanism operating in the phototransduction cascade of cones has been reported to affect visual sensitivity (Stockman, Langendörfer, Smithson, & Sharpe, 2006). This mechanism tends to increase cone sensitivity above low photopic luminances and under steady adaptation fields (Baker, 1949).

4.1.4. Spatial summation

Ricco's law states that, below a certain critical retinal area, ΔL-values are inversely proportional to the stimulated region. Consequently, detection thresholds for a 2° test are lower than those for a 0.45° test. In fact, this can be demonstrated when comparing the left and center panels in Fig. 1.

4.2. Influence of background/test sizes

The mechanisms included in our model can explain the detection thresholds that were measured under the three different background/test size conditions. We obtained contrast gains for our experimental conditions by interpolating Murray and Plainis's data (2003) to our luminances and eccentricities. We assumed that the fundamental spatial frequencies corresponding to 0.45° and 2° test sizes were around 1 c/deg and 0.25 c/deg, respectively. As reported by Murray and Plainis, contrast gain variations were negligible for spatial frequencies lower than 2 c/deg. Regarding the subtractive mechanism, the parameter, K_s, depending on both eccentricity and background size, was selected as the free parameter in the photopic range ($15 \text{ cd/m}^2 < L_b < 110 \text{ cd/m}^2$). This parameter, K_s, which modulates the feedback effect between cones and horizontal cells, was free to change with eccentricity and adaptation field size, but not with background luminance. In our model, g_c and g_r represent the effect of cone and rod gain control mechanisms, respectively. Data from physiological studies were used in our model (Dunn et al., 2006, 2007), weighted by the relative cone (a) and rod ($1-a$) contributions. These weighting coefficients changed with background luminance and eccentricity (Raphael & Macleod, 2011). A molecular mechanism was also considered (Baker, 1949; Stockman et al., 2006); it showed some influence in our model by slightly lowering the calculated thresholds when background luminances were higher than 80 cd/m². This molecular mechanism is a cellular mechanism in the receptor cell that adjusts its operating range to conform to the ambient illumination, and operates in this range of luminances (Valeton & Van Norren, 1983). The additive effect of all these gain components represents the background gain (see Eq. (A.6) in the Appendix A). Finally, the difference between luminance thresholds measured with test sizes of 2° and 0.45° have been explained by the effect of spatial summation, represented in the model by the parameter K (see Appendix A, Eq. (A.9)). In Fig. 3, the observer-averaged *tvi* data at the six retinal locations are plotted, as well as the model fitted to the data.

4.2.1. Background/test 10°/2°

As pointed out in Fig. 1, which shows the individual data, the triangles in Fig. 3 confirmed that Weber's law was fairly well followed in this background/stimulus size condition. The fitting procedure for this set of data consisted simply of calculating, for each eccentricity, the K_s-value that replicated our experimental threshold at $L_b = 60 \text{ cd/m}^2$. This simple procedure also allowed the model (solid line) to reproduce the measured thresholds in the mesopic range very finely. In fact, the standard deviations of the experimental data relative to the calculated ones in the mesopic range were between 0.04 and 0.17 log units for the different eccentricities. The goodness of fit of our model for this condition was very good ($\chi^2 > 0.997$ for all the eccentricities). The K_s-values, as a function of eccentricity, are plotted in Fig. 4 with solid squares indicating the average measurements of the three subjects. This parameter, as well as the effect of the subtractive mechanism, increased with increasing eccentricity. This behavior is well correlated with
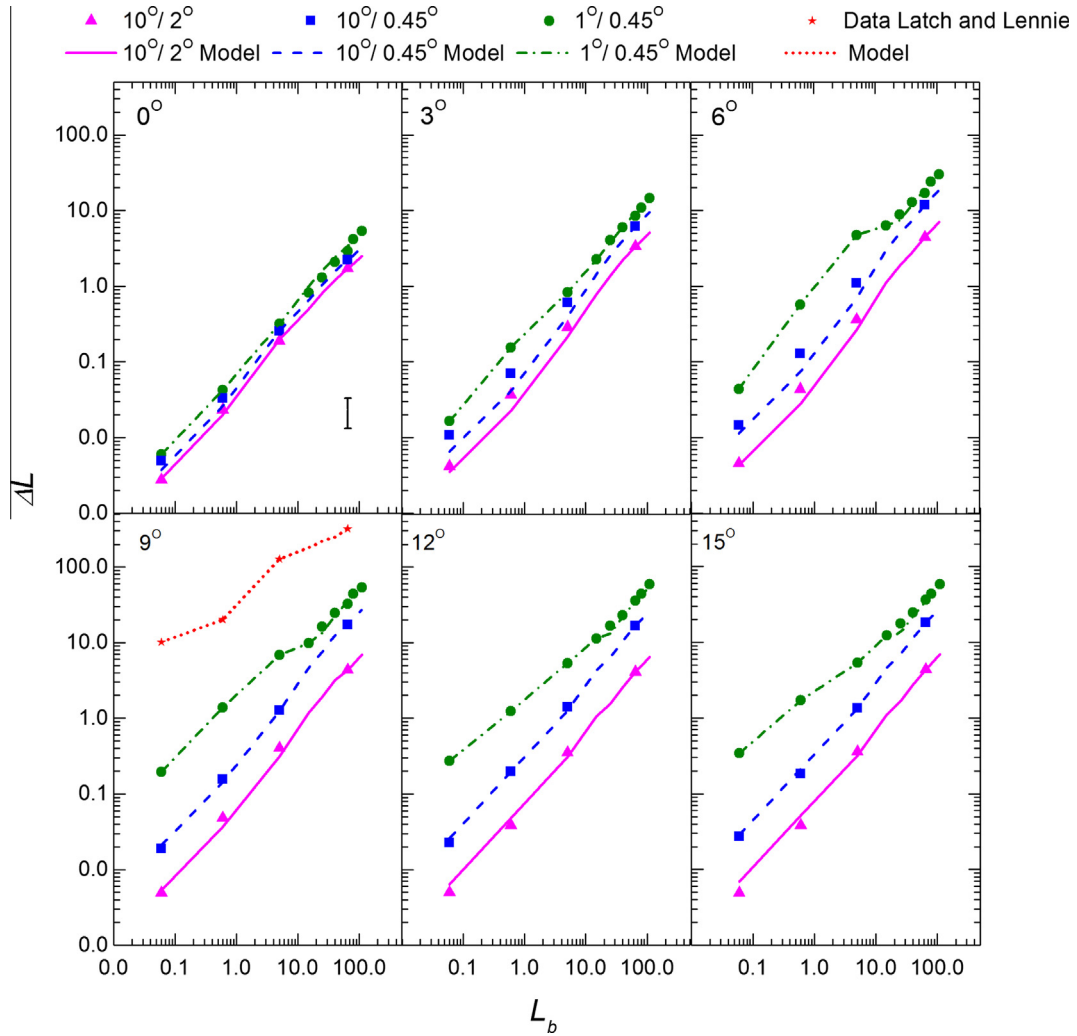
Fig. 3. Data (points) and predicted ΔL-values (continuous line for background/test 10°/2°; dashed line for background/test 10°/0.45°, dash-dotted line for 1°/0.45°) are plotted as a function of L_b (cd/m^2) for each eccentricity (both in log scale). The experimentally estimated uncertainty (±0.15 log units) is displayed in the first panel. Continuous and dashed lines run parallel to each other but with an increasing difference with eccentricity. However, dash-dotted line shows a greater increment in luminance thresholds for mesopic backgrounds than for photopic ones. Experimental data measured by Latch and Lennie (1977) are also displayed at the 9° eccentricity panel.
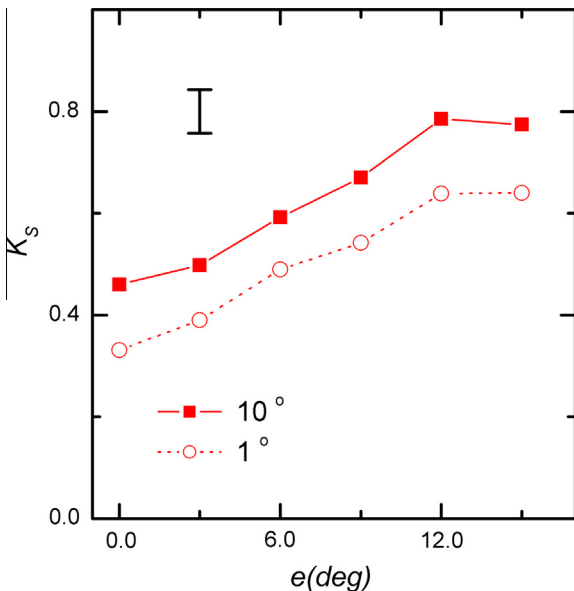

Fig. 4. K_s-values as a function of eccentricity for the average measurements of the three subjects, and both 10° and 1° background fields.

increasing horizontal cell dendritic size observed with increasing eccentricities (Rodieck, 1998; Wässle, Boycott, & Röhrenbeck, 1989). The error bar shown in the left panel of this figure represents a typical example of a 95% confidence interval. It was obtained according to the following. Random variations of the measured ΔL-value around the experimental uncertainty of ±0.15 log units were simulated and the corresponding K_s-values were obtained. Two standard deviations defined the plotted error bar.

4.2.2. Background/test 10°/0.45°

Squares in Fig. 3 show that, when the test size was reduced to 0.45°, *tvi* data moved upwards. This displacement was very similar, in log scale, for all background luminances and was larger for increasing eccentricities. This constancy in the threshold ratio was consistent with that found by Barlow (1958) for our range of background luminances, test angular sizes (2° and 0.45°) and test durations (40 ms), see Fig. 3 in Barlow (1958). The parameter K of the spatial summation mechanism allowed accounting for ΔL-values measured at these two stimuli size conditions. Starting from the model designed for the 10°/2° condition ($K = 1$), we recalculated K for each eccentricity in such a way that the model (dashed line) replicated the measured values (squares) at 60 cd/m^2. Once more, the model also fitted very well to the experimental thresh-
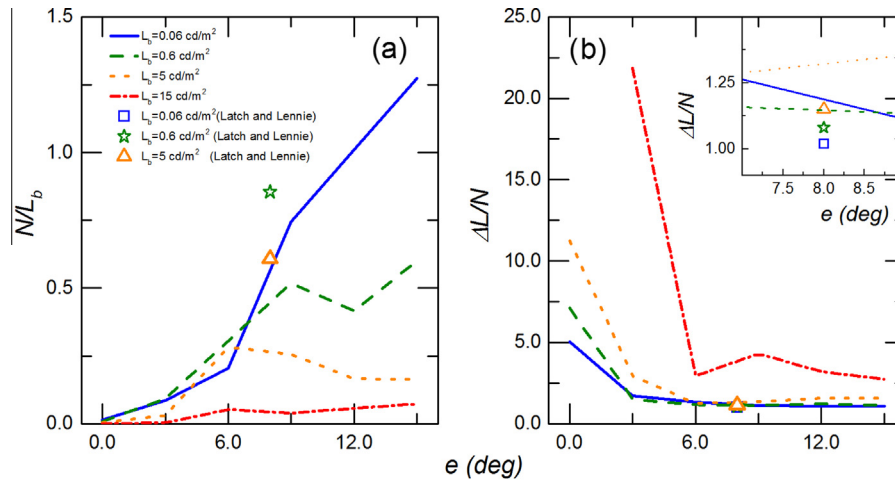
Fig. 5. (a) Variation of the ratio N/L_b as a function of eccentricity. (b) Variation of the signal-to-noise ratio as a function of eccentricity. Both figures have been plotted for the different mesopic background luminances under the 1°/0.45° condition. The values obtained when the model is fitted to Latch and Lennie (1977) data, measured at 8° eccentricity, are also included.

olds in the mesopic range. In all eccentricities the goodness of fit (χ^2) was higher than 0.968. The increments observed in K with increasing eccentricities are in agreement with previous studies (Barlow, 1958; Zuidema, Verschuure, Bouman, & Koenderink, 1981). These results will be commented on below.

4.2.3. Background/test 1°/0.45°

Fig. 3 also shows averaged ΔL-values measured for small background and test field sizes (circles). When reducing the background field from 10° to 1°, *tvi* curves moved upwards again. This threshold increment in the photopic range can be ascribed either to the influence of background field size on the control gain (Tyler & Liu, 1996), or to the reduction in the subtractive mechanism (Hayhoe et al., 1992). We have followed this second hypothesis. Therefore, starting from the model adapted to the 10°/0.45° condition, the parameter K_s was recalculated for each eccentricity (open circles in Fig. 4). Since more data were available in the photopic range for this background/test field size condition, the new K_s-value was the one that minimized the standard deviation between the predicted and measured ΔL-values in this range. The standard deviations of the calculated data relative to the experimental data in the photopic range were between 0.02 log units and 0.10 log units for all eccentricities. Although this approach was sufficient for the model to explain the photopic data, in the mesopic range the elevation of thresholds was much more significant, especially for eccentricities $\geqslant 6°$ (right column, Fig. 1). This elevation can be attributed to an increase in visual noise or to a reduction in retinal gain control triggered by visual noise. A simple way to fit the model to these data in the range 0.06 cd/m² < L_b < 15 cd/m² was to introduce a noise term N which affects the test detection and let it vary freely for each mesopic luminance and eccentricity in such a way that the model fits the experimental thresholds (Eq. (A.8)). For all eccentricities the goodness of fit (χ^2) was higher than 0.98.

The variation of the N/L_b ratio as a function of eccentricity for the background luminances in the range 0.06 < L_b < 15 cd/m² is shown in Fig. 5a. The ratio N/L_b tended to increase with eccentricity in a more remarkable way for the lowest L_b-values. Interestingly this ratio had some relative maximum values for 0.6 and 5 cd/m² at 9° and 6° respectively. In Fig. 5b we also plotted the signal-to-noise ratio $\Delta L/N$ as a function of eccentricity for the background luminances in the range 0.06 < L_b < 15 cd/m². As it is shown in this figure the highest values of this ratio were obtained, at all eccen-

tricities, for the highest background luminance. In all cases, this ratio reached the highest value in fovea, whereas it looks constant within the range 0.06 < L_b < 5 cd/m² for all off-axis eccentricities. The model results are plotted in Fig. 3.

4.3. Fit to Latch and Lennie (1977) data

In order to test the ability of this model to explain results obtained by other authors in similar experiments, we fitted the model to experimental thresholds obtained by Latch and Lennie (1977) in a rod-cone interaction experiment (Fig. 3, panel for 9°). The experimental data employed concerned the thresholds obtained by stimulating the peripheral retina at 8° eccentricity with a short-wavelength background field of 34′ angular size in order to analyze rod influence on the detection of spots 10′ in angular size presented for 10 ms.

We have fitted our model to the Latch and Lennie's data in the photopic range using the same procedure as with our data. In order to do this, we considered the retinal gain control information provided by Dunn et al. (2006, 2007). Since the background field size was very similar, we employed the same K_s-value we obtained for the 1°/0.45° combination at 9° eccentricity (see open circles in Fig. 4). The constant, K, accounts not only for spatial summation, but also temporal summation differences, and has been recalculated to obtain values compatible with those measured by Barlow (1958). As with our data, in the mesopic range we added a noise contribution in the modeling. On one hand, Fig. 5a contains the N/L_b ratio to optimize the model to Latch and Lennie (1977) results. As can be seen, their N/L_b-values were much higher than ours for the 1°/0.45° combination, particularly for L_b = 0.06 cd/m² where N/L_b = 4.2 (not included in the Fig. 5a. This significant effect of noise N that corresponds with significantly greater thresholds could be caused by the nature of the spectral power distribution of the background field employed in their experiment, which enhanced rod stimulation and therefore rod-cone interaction effects. It is interesting to remark that signal-to-noise ratio corresponding to Latch and Lennie's data agree very well with ours as shown in the inset in Fig. 5b.

5. Discussion and conclusions

Much progress has been made in the past regarding understanding *tvi* curves. However, these studies have usually been per-

formed at a particular retinal location, for a restricted interval of background luminances, or for a unique combination of background/test field sizes. Our work provided experimental *tvi* curves and an explanatory model that covered more than three orders of magnitude of background luminances (including mesopic and photopic ranges), retinal eccentricities from the fovea to 15°, and three different background/test field size combinations.

The main mechanisms explored with the model developed in this work were contrast gain, retinal gain control, and a subtractive mechanism. Most of the behavioral characteristics of these mechanisms have been described in the existing literature. These mechanisms underlie the threshold values measured when 0.06 cd/m^2 < L_b < 110 cd/m^2, for all eccentricities, and at 10°/2° background/test field sizes (see triangles and the solid line in Fig. 3). The K_s parameter, which changes the strength of the subtractive effect, was set to vary freely with changes in eccentricity in the photopic range. Since this mechanism considers the feedback existing between cones and horizontal cells (Wilson, 1997), it has been quantified in such a way that the model fits our threshold values at L_b = 60 cd/m^2, where the rod contribution is negligible. The same procedure has been employed for the 1°/0.45° background/test field combination. In Fig. 4, we can see how K_s changes with eccentricity and background field sizes. In fact, this influence of the background field size on the subtractive mechanism strength was pointed out by Burkhardt (1995). The explanation for this psychophysical effect can be related to the underlying physiology (Klaassen et al., 2012; VanLeeuwen et al., 2009). Although the horizontal cell density increases slightly with eccentricity up to 3°, and afterwards decreases, our measured K_s-parameters increase with eccentricity in a very similar way to how the dendritic field size increases in these cells (Rodieck, 1998). Furthermore, some studies on the primate retina have shown an increase in the horizontal cell receptive fields with eccentricity (Wässle et al., 1989). This would explain the results shown in Fig. 4.

For all these background luminance ranges, when the test size was reduced from 2° to 0.45°, threshold values increased due to a lack of spatial summation (see squares and the dashed line in Fig. 3). According to our measurements, this increment was higher for increasing eccentricities, but was independent of background luminances. As pointed out previously, this result was consonant with measurements performed by Barlow (1958) at these background luminances and for this range of angular test sizes and test durations. In a recent work, Kao and Chen (2012) quantified this effect of test size and eccentricity on thresholds and related it to receptive field sizes. Another recent work, performed at a cortical level, showed that the receptive field sizes increased with increasing eccentricity (Dumoulin & Wandell, 2008).

Threshold values increased when the background field size was reduced from 10° to 1°. This increment was particularly important at higher eccentricities and at lower background luminances; i.e., in those conditions where rod contributions to adaptation and/or detection were more significant. This has also been observed by other authors (Buck et al., 1979; Latch & Lennie, 1977; Temme & Frumkes, 1977). In the photopic range, this increment could be explained by a decrease in the subtractive mechanism strength. However, in the mesopic range, additional effects must be involved. Two different explanations have been offered in the literature for the increment in *tvi* curves in the mesopic range; i.e., a decrease in retinal gain or an increase in visual noise (Barlow, 1957; Shapley & Enroth-Cugell, 1984). The first explanation assumes that increasing luminances in the visual field produce changes in the retinal properties leading to adaptation. The second explanation assumes that quanta fluctuations may produce increments in luminance thresholds, particularly at low light levels. The debate currently continues, but more modern theories are attempting to combine both explanations (Brown & Rudd, 1998;

Rieke & Rudd, 2009; Schwartz & Rieke, 2013). In these experimental conditions our model explains the increase thresholds as a result of a significant increment of noise which affects directly to test detection, or indirectly through a decrease in the retinal gain control (see Eq. (A.8)). In fact, other authors have observed an increase in visual noise at lower background luminances (Schwartz & Rieke, 2013).

On the one hand, the anomalous increase of luminance thresholds in the mesopic range only for the 1°/0.45° conditions, but not for the 10° background size is in agreement with previous experiments like those performed by Aguilar and Stiles (1954) with a 20° background size and a 9° test size at 9° of eccentricity. They did not find these threshold elevations. On the other hand, Fig. 5a shows that noise effects were reduced significantly for the 1/0.45° condition as background luminance increased (L_b = 15 cd/m^2). In this background luminance condition, $\Delta L/N$ tends to increase significantly for all retinal eccentricities (Fig. 5b), which seems to point out that -in terms of adaptation- a larger size in a mesopic background field (10°) produces an inhibitory effect on noise in a similar way as it is produced with a smaller background field size (1°) at photopic luminances, though different causes could be involved. In fact, in experiments conducted under small background field sizes, lower than 2° (Bauer, Frumkes, & Holstein, 1983; Bauer, Frumkes, & Nygaard, 1983; Latch & Lennie, 1977), significantly increased luminance thresholds were obtained in the mesopic range at off-axis locations.

Note that in our experiment we have not attempted to perform spectrally selective stimulation of rods or cones. As can be seen in Fig. 5a an increase in the N/L_b ratio with eccentricity is observed, which is more relevant for the lowest background luminances. We hypothesize that the relative maxima observed in this figure for 5 and 0.6 cd/m^2 at 6° and 9° of eccentricity respectively might be due to rod-cone interaction effects. In an experiment where spectral stimulation of rods is intended (Latch & Lennie, 1977), the obtained N/L_b-values were much higher than ours at these background luminances and eccentricities. In fact, in another experiment with spectral selection of the stimulated background Bauer, Frumkes, and Nygaard (1983); Bauer, Frumkes, and Holstein (1983) developed a model that attributed these threshold elevations to rod-cone interactions, which could be explained in terms of a noise mechanism. Their model included an inhibitory spatial summator operator whose strength increased significantly with increasing background size and whose effect was to cancel any rod influence on cone detection thresholds for backgrounds greater than 2°. Following to Bauer et al. reasoning, we hypothesize that the increasing N/L_b-values for all mesopic background luminances, particularly for the lowest ones (solid curve in Fig. 5a) were due to increasing rod contribution.

More interesting conclusions arise from the analysis of Fig. 5b. The increasing signal-to-noise ratio observed in fovea with increasing background luminances reveals that, at this retinal location detection is limited mostly by the classical adaptation mechanisms: contrast gain, retinal gain control, etc. In this situation cones are the photoreceptors primarily involved in the whole process. At off-axis locations the very low $\Delta L/N$ values reached at 6° eccentricity for all mesopic luminances, seems to indicate that detection is mainly conditioned by noise, i.e. noise N is the most relevant limiting mechanism of the visual sensitivity. Since noise increases with eccentricity, as shown in Fig. 5a, it is reasonable that these signal-to-noise ratios keep constant and close to unity for further eccentricities and for all mesopic background luminances. In fact, this argument would also explain why the $\Delta L/N$ values calculated from data obtained in the Latch and Lennie's experiment were even lower than ours. Once more, in this experiment rod contribution to adaptation is enhanced by selective spectral stimulation which would produce greater noise effects according to our previous argument.

When analyzing the way the noise term N has been introduced in our model (see Eq. (A.4)), one can attribute the observed effects directly to noise or indirectly to a retinal gain control decrease triggered by noise during the test presentation. Such interpretation is not new (Brown & Rudd, 1998; Donner, Copenhagen, & Reuter, 1990; Rieke & Rudd, 2009; Schwartz & Rieke, 2013). In those experimental conditions dominated by cones (photopic luminances or foveal detection), cone gain control is fast enough to change during the 40 ms the test is presented in such a way that noise effects are minimized. Opposite, at off-axis eccentricities and at mesopic luminances levels, rod gain control cannot be activated during test presentation due to their slower nature (Barbur, 1982; Cao, Zele, & Pokorny, 2007; MacLeod, 1972; Sharpe, Stockman, & MacLeod, 1989; Sun, Pokorny, & Smith, 2001; Van den Berg & Spekreijse, 1977; Zele, Maynard, & Feigl, 2013). In these conditions visual noise cannot be inhibited. These effects are not appreciated when the background field size is increased up to 10°, since the subtractive mechanism and gain control are intense enough to compensate noise effects. In any case, this experiment was not designed to elucidate between the involvement of visual noise or the gain control variation triggered by noise.

As a final conclusion, the model developed in this work was able to explain the measured detection luminance thresholds by considering and quantifying the different mechanisms involved when a change in the background luminance, eccentricity, or background/test size was produced. The subtractive mechanism strength was more significant for increasing eccentricities and for higher background field sizes. The spatial summation was not complete for 0.45° test sizes and this lack of summation increased with increasing eccentricities. According to our model, visual noise or a retinal gain control triggered by visual noise play an important role in the elevation of luminance thresholds in the mesopic range for 1° background fields.

Disclosure

The authors report no conflicts of interest and have no proprietary interest in any of the materials mentioned in this article.

Acknowledgments

Appendix A

The model employed in this study predicted luminance threshold values; i.e., ΔL. It was based on a previous model developed by Barrionuevo et al. (2013). ΔL-values come from the Weber contrast expression (Eq. (A.1)). It is assumed, as usual, that the minimum Weber contrast necessary for detection, C_n, is at least that corresponding to the visual noise ($C_n = 0.01$).

$$C_n = \frac{L_T - L_b}{L_b} = \frac{\Delta L}{L_b} \tag{A.1}$$

However, in order to analyze the mechanisms involved in the visual adaptation process, luminance values are substituted in Eq. (A.1) by cell responses to the light levels involved (Eq. (A.2)) (Shapley & Enroth-Cugell, 1984):

$$C_n = G_c \frac{R(L_T) - R(L_b)}{R(L_b)} \tag{A.2}$$

with L_T and L_b as the test and background luminances, respectively, and G_c as the contrast gain involved, whose values for the different eccentricities and luminances have been taken by interpolation from those measured by Murray and Plainis (2003). In Eq. (A.2), we called $R(L_b)$ and $R(L_T)$ as the responses to background and test luminances, respectively. They can be obtained from the Naka-Rushton expression (Naka & Rushton, 1966):

$$R(L_b) = \frac{1}{1 + \left[\frac{\sigma}{g_b(L_b - S)}\right]^n} \tag{A.3}$$

$$R(L_T) = \frac{1}{1 + \left[\frac{\sigma}{g_T(L_T - S - N)}\right]^n} \tag{A.4}$$

In Eqs. (A.3) and (A.4), σ and n represent the half-saturation constant and the Hill constant, respectively. These constants were taken from Adelson (1982). N represents a visual noise term which appears in the detection process and is allowed to take non null values only in the mesopic range of background luminances and for all off-axis eccentricities. S represents the subtractive mechanism, which reduces the background luminance. According to previous proposals (Barrionuevo, Colombo, & Issolio, 2013). S is given by:

$$\frac{dS}{dt} + \frac{g_m}{\tau} S = K_s L_b \frac{g_m}{\tau} \tag{A.5}$$

In Eq. (A.5) t represents the exposure time, τ is a constant time, g_m is the factor that modifies the speed of the mechanism to reach a stable state, and K_s is a value related to the feedback signal coming from the horizontal cells (Wilson, 1997). In this work, we assumed that the parameter K_s depends on both eccentricity and background adaptation size. In Eqs. (A.3) and (A.4), g_b represent the retinal gain control for the background. It informs the combined effect of cone and rod responses to luminous stimulus according to:

$$g_b = g_c a M + g_r (1 - a) \tag{A.6}$$

where g_r and g_c are the rod and cone gain controls, respectively (Dunn, Lankheet, & Rieke, 2007; Dunn et al., 2006) and a is the relative cone contribution (Raphael & Macleod, 2011). In Eq. (A.6), M represents a molecular mechanism affecting the cone gain control. This mechanism appears in steady adaptation fields at low photopic luminances (Stockman et al., 2006). This is given by the expression:

$$M = \frac{1}{1 + \left(\frac{L_b}{L_i}\right)^n} \tag{A.7}$$

where L_i is the luminance where M reaches its half value.

Finally, ΔL is obtained by substituting all terms defined in Eqs. (A.3) to (A.7) in Eq. (A.2).

$$\Delta L = \left(\frac{\sigma_T'^n}{\frac{1}{\left[\frac{C_n}{G_c}R(L_b)\right] + R(L_b)} - 1}\right)^{1/n} + S + N - L_b \tag{A.8}$$

In cases where spatial summation is not complete (test size 0.45°), $\Delta L_{0.45°}$ can be related to $\Delta L_{2°}$ by simply multiplying by a constant K, which depends on eccentricity but not on background luminance.

Table A1

Values employed for the different parameters and constants used in the model. The values or the bibliographic source are indicated. In those cases where the parameter has been used as a free parameter to fit the model to the experimental data, an explanation is provided.

Magnitude	Employed value or bibliographic source
Contrast gain data G_c	Murray and Plainis (2003)
Half saturation constant σ	0.2 cd/m^2
Hill constant n	1.0
Cone gain control g_c	Dunn et al. (2007)
Rod gain control g_r	Dunn et al. (2006)
Relative cone contribution a	Raphael and Macleod (2011)
L_i (molecular mechanism)	80 cd/m^2
g_m, τ	Barrionuevo et al. (2013)
K_s	Free parameter used to fit the model to the subset of photopic data (60 cd/m^2) in case of 10°/2° and 10°/0.45° combinations, and between 25 and 110 cd/m^2 for 1°/0.45°), see Fig. 4
N	Free parameter used to fit the model to the subset of mesopic data in case of the 1°/0.45° field sizes combination
K	Free parameter, dependent on eccentricity, used to relate threshold luminances measured under 10°/2° and 10°/0.45° field sizes combinations

$$\Delta L_{0.45°} = K \Delta L_{2°} \tag{A.9}$$

Finally, a summary of the specific values employed in the model for the different magnitudes considered or the bibliographic sources they were taken from, are listed in Table A1

References

Adelson, E. H. (1982). Saturation and adaptation in the rod system. *Vision Research, 22*(10), 1299–1312. http://dx.doi.org/10.1016/0042-6989(82)90143-2.

Aguilar, M., & Stiles, W. S. (1954). Saturation of the rod mechanism of the retina at high levels of stimulation. *Journal of Modern Optics, 1*(1), 59–65. http://dx.doi.org/10.1080/713818657.

Baker, H. D. (1949). The course of foveal light adaptation measured by the threshold. *Journal of the Optical Society of America, 39*(2), 172–179. http://dx.doi.org/10.1364/JOSA.39.000172.

Barbur, J. L. (1982). Reaction-time determination of the latency between visual signals generated by rods and cones. *Ophthalmic and Physiological Optics, 2*(3), 179–185. http://dx.doi.org/10.1111/j.1475-1313.1982.tb00175.x.

Barlow, H. B. (1957). Noise and the visual threshold. *Nature, 180*(4599), 1405. http://dx.doi.org/10.1038/1801405a0.

Barlow, H. B. (1958). Temporal and spatial summation in human vision at different background intensities. *Journal of Physiology – London, 141*(2), 337–350. http://dx.doi.org/10.1113/jphysiol.1958.sp005978.

Barlow, H. B. (1965). Optic nerve impulses and Weber's law. *Cold Spring Harbor Symposia on Quantitative Biology, 30*, 539–546. http://dx.doi.org/10.1101/SQB.1965.030.01.052.

Barrionuevo, P. A., Colombo, E. M., & Issolio, L. A. (2013). Retinal mesopic adaptation model for brightness perception under transient glare. *Journal of the Optical Society of America A: Optics, Image Science, and Vision, 30*(6), 1236–1247. http://dx.doi.org/10.1364/JOSAA.30.001236.

Bauer, G. M., Frumkes, T. E., & Nygaard, R. W. (1983a). The signal-to-noise characteristics of rod-cone interaction. *Journal of Physiology – London, 337*, 101–119. http://dx.doi.org/10.1113/jphysiol.1983.sp014614.

Bauer, G. M., Frumkes, T. E., & Holstein, G. R. (1983b). The influence of rod light and dark adaptation upon rod-cone interaction. *Journal of Physiology – London, 337*, 121–135. http://dx.doi.org/10.1113/jphysiol.1983.sp014615.

Buck, S. L., Peeples, D. R., & Makous, W. (1979). Spatial patterns of rod-cone interaction. *Vision Research, 19*(7), 775–782. http://dx.doi.org/10.1016/0042-6989(79)90153-6.

Brown, L. G., & Rudd, M. E. (1998). Evidence for a noise gain control mechanism in human vision. *Vision Research, 38*(13), 1925–1933. http://dx.doi.org/10.1016/S0042-6989(97)00400-8.

Buck, S. L. (2004). Rod-cone interactions in human vision. In L. M. Chalupa & J. S. Werner (Eds.). *The Visual Neuroscience* (Vol. 1, pp. 863–878). Cambridge: MIT Press Mass.

Buck, S. L. (2014). The interaction of rod and cone signals: Pathways and psychophysics. In J. S. Werner & L. M. Chalupa (Eds.), *The new visual neurosciences* (pp. 485–497). Cambridge: MIT Press Mass.

Burkhardt, D. A. (1995). The influence of center-surround antagonism on light adaptation in cones in the retina of the turtle. *Visual Neuroscience, 12*(5), 877–885. http://dx.doi.org/10.1017/S0952523800009433.

Cao, D., Zele, A. J., & Pokorny, J. (2007). Linking impulse response functions to reaction time: Rod and cone reaction time data and a computational model. *Vision Research, 47*(8), 1060–1074. http://dx.doi.org/10.1016/j.visres.2006.11.027.

Cao, D., & Pokorny, J. (2010). Rod and cone contrast gains derived from reaction time distribution modeling. *Journal of Vision, 10*(2), 1–15. http://dx.doi.org/10.1167/10.2.11.

Croner, L. J., & Kaplan, E. (1994). Receptive fields of P and M ganglion cells across the primate retina. *Vision Research, 35*(1), 7–24.

Crook, J. D., Packer, O. S., Troy, J. B., & Dacey, D. M. (2014). Synaptic mechanisms of color and luminance coding: Rediscovering the X–Y-cell dichotomy in primate retinal ganglion cells. In J. S. Werner & L. M. Chalupa (Eds.), *The new visual neurosci* (pp. 123–144). Cambridge: MIT Press Mass.

Curcio, C. A., Sloan, K. R., Kalina, R. E., & Hendrickson, A. E. (1990). Human photoreceptor topography. *Journal of Comparative Neurology, 292*(4), 497–523. http://dx.doi.org/10.1002/cne.902920402.

Demb, J. B. (2008). Functional circuitry of visual adaptation in the retina. *Journal of Physiology, 586*, 4377–4384. http://dx.doi.org/10.1113/jphysiol.2008.156638.

Donner, K., Copenhagen, D., & Reuter, T. (1990). Weber and noise adaptation in the retina of the toad *Bufo marinus. Journal of General Physiology, 95*, 733–753. http://dx.doi.org/10.1085/jgp.95.4.733.

Donner, K. (1992). Noise and the absolute thresholds of cone and rod vision. *Vision Research, 32*, 853–866. http://dx.doi.org/10.1016/0042-6989(92)90028-H.

Dumoulin, S. O., & Wandell, B. A. (2008). Population receptive field estimates in human visual cortex. *NeuroImage, 39*(2), 647–660. http://dx.doi.org/10.1016/j.neuroimage.2007.09.034.

Dunn, F. A., Doan, T., Sampath, A. P., & Rieke, F. (2006). Controlling the gain of rod-mediated signals in the mammalian retina. *Journal of Neuroscience, 26*(15), 3959–3970. http://dx.doi.org/10.1523/JNEUROSCI.5148-05.2006.

Dunn, F. A., Lankheet, M. J., & Rieke, F. (2007). Light adaptation in cone vision involves switching between receptor and post-receptor sites. *Nature, 449*, 603–606. http://dx.doi.org/10.1038/nature06150.

Freeman, D. K., Graña, G., & Passaglia, C. L. (2010). Retinal ganglion cell adaptation to small luminance fluctuations. *Journal of Neurophysiology, 104*(2), 704–712. http://dx.doi.org/10.1152/jn.00767.2009.

Garway-Heath, D. F., Caprioli, J., Fitzke, F. W., & Hitchings, R. A. (2000). Scaling the hill of vision: The physiological relationship between light sensitivity and ganglion cell numbers. *Investigative Ophthalmology & Visual Science, 41*(7), 1774–1782.

Heine, W. F., & Passaglia, C. L. (2011). Spatial receptive field properties of rat retinal ganglion cells. *Visual Neuroscience, 28*(5), 403–417. http://dx.doi.org/10.1017/S0952523811000307.

Hayhoe, M. M., Benimoff, N. I., & Hood, D. C. (1987). The time-course of multiplicative and subtractive adaptation process. *Vision Research, 27*(11), 1981–1996. http://dx.doi.org/10.1016/0042-6989(87)90062-9.

Hayhoe, M. M., Levin, M. E., & Koshel, R. J. (1992). Subtractive processes in light adaptation. *Vision Research, 32*(2), 323–333. http://dx.doi.org/10.1016/0042-6989(92)90142-6.

Hood, D., & Finkelstein, M. (1986). Sensitivity to light. In K. Boff, L. Kaufman, & J. Thomas (Eds.), *Handbook of perception and human performance* (Vol. 1, pp. 5.1–5.66). New York: Wiley-Interscience.

Jarsky, T., Cembrowski, M., Logan, S. M., Kath, W. L., Riecke, H., Demb, J. B., & Singer, J. H. (2011). A synaptic mechanism for retinal adaptation to luminance and contrast. *Journal of Neuroscience, 31*(30), 11003–11015. http://dx.doi.org/10.1523/JNEUROSCI.2631-11.2011.

Joselevitch, C., & Kamermans, M. (2013). Gain control in the outer retina. In *Proceedings of the 10th international congress on cell biology* (pp. 153–157).

Kao, C., & Chen, C. (2012). Seeing visual word forms: Spatial summation, eccentricity and spatial configuration. *Vision Research, 62*, 57–65. http://dx.doi.org/10.1016/j.visres.2012.03.015.

Klaassen, L. J., Fahrenfort, I., & Kamermans, M. (2012). Connexin hemichannel mediated ephaptic inhibition in the retina. *Brain Research, 1487*, 25–38. http://dx.doi.org/10.1016/j.brainres.2012.04.059.

Latch, M., & Lennie, P. (1977). Rod cone interaction in light adaptation. *Journal of Physiology – London, 269*, 517–534. http://dx.doi.org/10.1113/jphysiol.1977.sp011912.

MacLeod, D. I. (1972). Rods cancel cones in flicker. *Nature, 235*(5334), 173–174.

Matesanz, B. M., Issolio, L., Arranz, I., De la Rosa, C., Menéndez, J. A., Mar, S., & Aparicio, J. A. (2011). Temporal retinal sensitivity in mesopic adaptation. *Ophthalmic and Physiological Optics, 31*(6), 615–624. http://dx.doi.org/10.1111/j.1475-1313.2011.00859.x.

Murray, I. J., & Plainis, S. (2003). Contrast coding and magno/parvo segregation revealed in reaction time studies. *Vision Research, 43*(25), 2707–2719. http://dx.doi.org/10.1016/S0042-6989(03)00408-5.

Naka, K. I., & Rushton, W. A. (1966). S-potentials from colour units in the retina of fish (Cyprinidae). *Journal of Physiology – London, 185*(3), 536–555. http://dx.doi.org/10.1113/jphysiol.1966.sp008001.

Osterberg, G. (1935). Topography of the layer of rods and cones in the human retina. *Acta Ophthalmologica Supplement, 13*(6), 1–102.

Purpura, K., Kaplan, E., & Shapley, R. M. (1988). Background light and the contrast gain of primate P and M retinal ganglion cells. *Proceedings of the National Academy of Sciences of the United States of America, 85*(12), 4534–4537. http://dx.doi.org/10.1073/pnas.85.12.4534.

Raphael, S., & Macleod, D. I. A. (2011). Mesopic luminance assessed with minimum motion photometry. *Journal of Vision, 11*(9), 1–21. http://dx.doi.org/10.1167/11.9.1.

Redmond, T., Zlatkova, M. B., Vassilev, A., Garway-Heath, D. F., & Anderson, R. S. (2013). Changes in Ricco's area with background luminance in the S-cone pathway. *Optometry & Vision Sciences, 90*(1), 66–74. http://dx.doi.org/10.1097/OPX.0b013e318278fc2b.

Rieke, F., & Rudd, M. E. (2009). The challenges natural images pose for visual adaptation. *Neuron, 64*(5), 605–616. http://dx.doi.org/10.1016/j.neuron.2009.11.028.

Rodieck, R. W. (1998). *The first steps in seeing* (1st ed., pp. 231–234). Washington: Sinauer Associates Inc.

Schwartz, G. W., & Rieke, F. (2013). Controlling gain one photon at a time. *eLife, 2*, e00467. http://dx.doi.org/10.7554/eLife.00467.

Shapley, R., & Enroth-Cugell, C. (1984). Chapter 9 visual adaptation and retinal gain controls. *Progress in Retinal Research, 3*, 263–346. http://dx.doi.org/10.1016/0278-4327(84)90011-7.

Sharpe, L. T., Stockman, A., & MacLeod, D. I. (1989). Rod flicker perception: Scotopic duality, phase lags and destructive interference. *Vision Research, 29*(11), 1539–1559. http://dx.doi.org/10.1016/0042-6989(89)90137-5.

Smith, V. C., & Pokorny, J. (2003). Color matching and color discrimination. In S. K. Shevell (Ed.), *The science of color* (2nd ed., pp. 103–148). Amsterdam: Elsevier.

Snippe, H. P., Poot, L., & van Hateren, J. H. (2000). A temporal model for early vision that explains detection thresholds for light pulses on flickering backgrounds. *Visual Neuroscience, 17*(3), 449–462. http://dx.doi.org/10.1017/S0952523800173110.

Snippe, H. P., Poot, L., & van Hateren, J. H. (2004). Asymmetric dynamics of adaptation after onset and offset of flicker. *Journal of Vision, 4*(1), 1–12. http://dx.doi.org/10.1167/4.1.1.

Stockman, A., & Sharpe, L. T. (2006). Into the twilight zone: The complexities of mesopic vision and luminous efficiency. *Ophthalmic and Physiological Optics, 26*(3), 225–239. http://dx.doi.org/10.1111/j.1475-1313.2006.00325.x.

Stockman, A., Langendörfer, M., Smithson, H. E., & Sharpe, L. T. (2006). Human cone light adaptation: From behavioral measurements to molecular mechanisms. *Journal of Vision, 6*(11), 1194–1213. http://dx.doi.org/10.1167/6.11.5.

Stockman, A., Petrova, D., & Henning, G. B. (2014). Color and brightness encoded in a common L- and M-cone pathway with expansive and compressive nonlinearities. *Journal of Vision, 14*(3), 1–32. http://dx.doi.org/10.1167/14.3.1.

Sun, H., Pokorny, J., & Smith, V. C. (2001). Rod-cone interactions assessed in inferred magnocellular and parvocellular postreceptoral pathways. *Journal of Vision, 1*(1), 42–54. http://dx.doi.org/10.1167/1.1.5.

Temme, L. A., & Frumkes, T. E. (1977). Rod-cone interaction in human scotopic vision 3. Rods influence cone increment thresholds. *Vision Research, 17*(6), 681–685. http://dx.doi.org/10.1016/S0042-6989(77)80002-3.

Thoreson, W. B., & Mangel, S. C. (2012). Lateral interactions in the outer retina. *Progress in Retinal and Eye Research, 31*, 407–441. http://dx.doi.org/10.1016/j.preteyeres.2012.04.003.

Tyler, C. W., & Liu, L. (1996). Saturation revealed by clamping the gain of the retinal light response. *Vision Research, 36*(16), 2553–2562. http://dx.doi.org/10.1016/0042-6989(95)00298-7.

Valeton, J. R., & Van Norren, D. (1983). Light adaptation of primate cones – An analysis based on extracellular data. *Vision Research, 23*(12), 1539–1547. http://dx.doi.org/10.1016/0042-6989(83)90167-0.

Van den Berg, T. J., & Spekreijse, H. (1977). Interaction between rod and cone signals studied with temporal sine wave stimulation. *Journal of the Optical Society of America, 67*(9), 1210–1217. http://dx.doi.org/10.1364/JOSA.67.001210.

VanLeeuwen, M., Fahrenfort, I., Sjoerdsma, T., Numan, R., & Kamermans, M. (2009). Lateral gain control in the outer retina leads to potentiation of center responses of retinal neurons. *Journal of Neuroscience, 29*(19), 6358–6366. http://dx.doi.org/10.1523/JNEUROSCI.5834-08.2009.

Wässle, H., Boycott, B. B., & Röhrenbeck, J. (1989). Horizontal cells in the monkey retina: Cone connections and dendritic network. *European Journal of Neuroscience, 1*(5), 421–435. http://dx.doi.org/10.1111/j.1460-9568.1989.tb00350.x.

Wilson, H. R. (1997). A neural model of foveal light adaptation and afterimage formation. *Visual Neuroscience, 14*(3), 403–423. http://dx.doi.org/10.1017/S0952523800012098.

Zele, A. J., & Cao, D. (2015). Vision under mesopic and scotopic illumination. *Frontiers in Psychology, 5*, 1594. http://dx.doi.org/10.3389/fpsyg.2014.01594.

Zele, A. J., Maynard, M. L., & Feigl, B. (2013). Rod and cone pathway signaling and interaction under mesopic illumination. *Journal of Vision, 13*(1), 21. http://dx.doi.org/10.1167/13.1.21.

Zuidema, P., Verschuure, H., Bouman, M. A., & Koenderink, J. J. (1981). Spatial and temporal summation in the human dark-adapted retina. *Journal of the Optical Society of America, 71*(12), 1472–1480. http://dx.doi.org/10.1364/JOSA.71.001472.